



## **Mutations in Citron Kinase Cause Recessive Microlissencephaly with Multinucleated Neurons**

Brian N. Harding, Amanda Moccia, Séverine Drunat, Omar Soukarieh, Hélène Tubeuf, Lyn S. Chitty, Alain Verloes, Pierre Gressens, Vincent El ghouzzi, Sylvie Joriot, et al.

### **► To cite this version:**

Brian N. Harding, Amanda Moccia, Séverine Drunat, Omar Soukarieh, Hélène Tubeuf, et al.. Mutations in Citron Kinase Cause Recessive Microlissencephaly with Multinucleated Neurons. *American Journal of Human Genetics*, 2016, 99 (2), pp.511-520. <10.1016/j.ajhg.2016.07.003>. <hal-02324787>

**HAL Id: hal-02324787**

**<https://hal.science/hal-02324787v1>**

Submitted on 8 Jun 2020

**HAL** is a multi-disciplinary open access archive for the deposit and dissemination of scientific research documents, whether they are published or not. The documents may come from teaching and research institutions in France or abroad, or from public or private research centers.

L'archive ouverte pluridisciplinaire **HAL**, est destinée au dépôt et à la diffusion de documents scientifiques de niveau recherche, publiés ou non, émanant des établissements d'enseignement et de recherche français ou étrangers, des laboratoires publics ou privés.



HAL Authorization

1 **Mutations in *Citron-Kinase* a cause of autosomal recessive micro-lissencephaly with**  
2 **multinucleated neurons.**

3 Harding B<sup>1</sup>, Moccia A<sup>2</sup>, Drunat S<sup>3</sup>, Soukarieh O<sup>4</sup>, Tubeuf H<sup>5</sup>, Chitty L<sup>6</sup>, Verloes A<sup>3</sup>, Gressens  
4 P<sup>7</sup>, El Ghouzzi V<sup>8</sup>, Joriot S<sup>9</sup>, Di Cunto F<sup>10</sup>, Martins A<sup>11</sup>, Passemard S<sup>12</sup>, Bielas S. L.<sup>13\*</sup>

5  
6 Pathology and Laboratory Medicine, Perelman School of Medicine, University of Pennsylvania  
7 and Children's Hospital of Philadelphia, Philadelphia, PA 19104, USA.

8 <sup>2</sup> Department of Human Genetics, University of Michigan Medical School, Ann Arbor, MI 48109,  
9 USA.

10 <sup>3</sup> Département de Génétique, Protect, Hôpital Robert Debré, Paris 75019, France; INSERM  
11 U1141, Hôpital Robert Debré, Paris 75019, France.

12 <sup>4</sup> INSERM U1079, Institute for Research and Innovation in Biomedicine, University of Rouen,  
13 Normandy Centre for Genomic and Personalized Medicine, Rouen 76183, France.

14 <sup>5</sup> INSERM U1079, Institute for Research and Innovation in Biomedicine, University of Rouen,  
15 Normandy Centre for Genomic and Personalized Medicine, Rouen 76183, France; Interactive  
16 Biosoftware, Rouen 76000, France.

17 <sup>6</sup> Genetics and Genomic Medicine, UCL Institute of Child Health and Great Ormond Street NHS  
18 Foundation Trust, London WC1N 1EH, UK.

19 <sup>7</sup> INSERM U1141, Hôpital Robert Debré, Paris 75019, France; Université Paris Diderot, Hôpital  
20 Robert Debré, Paris 75019, France; Center for Developing Brain, King's College, St. Thomas'  
21 Campus, London WC2R 2LS, UK.

22 <sup>8</sup> INSERM U1141, Hôpital Robert Debré, Paris 75019, France.

23 <sup>9</sup> Service de Neuropédiatrie, Centre Hospitalier Régional Universitaire de Lille, Lille 59037,  
24 France.

25 <sup>10</sup> Department of Molecular Biotechnology and Health Sciences, University of Turin, Turin 10126,  
26 Italy.

27 <sup>11</sup> Interactive Biosoftware, Rouen 76000, France.

28 <sup>12</sup> Département de Génétique, Protect, Hôpital Robert Debré, Paris 75019, France; INSERM  
29 U1141, Hôpital Robert Debré, Paris 75019, France; Université Paris Diderot, Hôpital Robert  
30 Debré, Paris 75019, France.

31 <sup>13</sup> Department of Human Genetics, University of Michigan Medical School, Ann Arbor, MI 48109,  
32 USA. Electronic address: [sbielas@umich.edu](mailto:sbielas@umich.edu).

33 Conflict of interest: The authors have declared that no conflict of interest exists.

34 Keywords: Cytokinesis, Neurogenesis, Primary Microcephaly, Lissencephaly, Autosomal Recessive, Citron  
35 Kinase.

**Abstract:**

Primary microcephaly is a neurodevelopmental disorder caused by a reduction in brain size attributed to defects in early neurogenesis. Mutations in numerous genes encoding proteins that localize to the mitotic spindle and centrosome are implicated in the pathogenicity of primary microcephaly. In contrast, involvement of the contractile ring and midbody required for cleavage furrow constriction and abscission have not previously been implicated in primary microcephaly. Citron Kinase (CIT), a component of the mitotic contractile ring, is a multi-domain protein that localizes to the cleavage furrow and midbody of mitotic cells, where it is required for the completion of cytokinesis. Rodent models of *Cit* deficiency highlighted the role of this gene in neurogenesis and microcephaly over a decade ago. Here we identify recessively inherited pathogenic variants in *CIT* as the genetic basis of severe microcephaly and neonatal death. We present postmortem data showing that CIT is critical to build a normally sized human brain. Consistent with cytokinesis defects attributed to CIT, multinucleated neurons are observed throughout the cerebral cortex and cerebellum of an affected proband, expanding our understanding of mechanisms attributed to primary microcephaly.

**Main:**

Primary microcephaly is a genetically heterogeneous neurodevelopmental disorder characterized by a severe reduction in brain growth<sup>1</sup>. This decreased brain volume often stems from a primary defect in neurogenesis. The cerebral cortex is composed of neurons born from neural progenitor cells (NPCs) that reside adjacent to the lateral ventricle during early neurodevelopment<sup>2</sup>. The mitotic machinery of NPCs is critical not only for rapid expansion of the progenitor pool required for normal brain growth, but also for maintaining the balance between proliferation and differentiation. Human genetics has identified many primary microcephaly genes which impact the fidelity of mitotic spindle placement and centrosome stability required to build a human brain of normal size<sup>3-8</sup>. Surprisingly, other steps in mitosis have not been implicated by neurogenetics in the pathophysiology of microcephaly, despite a series of rodent models showing that cleavage furrow placement, constriction of the contractile ring and abscission by the midbody are critical for neurogenesis<sup>9-11</sup>.

CIT is a multi-domain protein that localizes to the cleavage furrow and midbody where it functions in cytokinesis and abscission, the final steps of mitosis (Fig. 1a)<sup>12,13</sup>. CIT facilitates protein-protein interactions between contractile ring components (with anillin, actin, myosin and RhoA) and has a N-terminal kinase domain, both of which are critical for abscission<sup>12,14,15</sup>. Studies in drosophila and mammals demonstrate the evolutionarily conserved function of *CIT* in cytokinesis, with mutations that disrupt abscission resulting in binucleate cells. The impact of cytokinesis defects on brain development and size are evident in the *Cit* knockout mouse and the *Flathead* rat with a spontaneous nonsense mutation in *Cit* exon 1. In rodents *Cit* is critical for proliferation of NPCs and male germ cell precursors. *Cit* null animals are characterized by testicular hypoplasia, microcephaly, ataxia, growth deficiencies and lethal epilepsy<sup>10,11</sup>. These phenotypes have been linked to cytokinesis defects and the presence of multinucleated cells throughout the cortex and cerebellum. Premature differentiation of early NPCs and widespread

apoptosis are compounded across development, resulting in a cerebral cortex and cerebellum less than 50% the size of normal brain. Cortical hypoplasia and layer disorganization are predicted to account for the recurrent spontaneous seizures and premature death in the mice<sup>16</sup>. Roles for *CIT* in human brain development and primary microcephaly have been predicted but not yet reported.

Here we describe three independent families, each with multiple affected children who presented with severe micro-lissencephaly associated with neonatal mortality (Fig. 1b). The clinical features of the probands are provided in Table 1. Egyptian Family A is consanguineous with two microcephalic male siblings. The first affected child died in the neonatal period (Fig. 1b). Proband A was delivered at term and weighed 2600 grams (-2SD) consistent with 5th percentile for growth. Head circumference, not measured until 3.5 months of age, was 27cm (-11 to -12 SD below the age/sex mean). His length at 3.5 months was 53 cm (-4 to -5 SD), and he continued to experience failure to thrive thereafter. Dysmorphisms were noted including hypotelorism, sloping forehead and large ears (Fig. 2a). He exhibited axial hypotonia, upper and lower extremity hypertonia, increased deep tendon reflexes and lack of head support. Microcephaly was confirmed by MRI, which also revealed lissencephaly, enlarged ventricles, agenesis of the corpus callosum, cerebellar hypoplasia and brainstem hypoplasia (Fig. 2b). T2 hyperintensity was also noted throughout the white matter consistent with spastic tetraplegia.

Family B has two affected children born to first cousin parents from United Arab Emirates. Male Proband B was noted by ultrasound at 30 gestational weeks (GWs) to have microcephaly, intrauterine growth retardation, and oligohydramnios. Echocardiogram indicated cardiomegaly, biventricular dilatation and tricuspid regurgitation. He was delivered by spontaneous vaginal delivery at 39 GWs with a head circumference of 24cm, 8 standard deviations below the age/sex mean, and a body length measurement of 27.2cm crown-rump (2.5 SD below the

mean) consistent with 36 GWs. Despite Apgar scores of 8 at one minute, and 9 at 5 minutes, he died the following day.

At birth, the brain weight of Proband B was 40g (10% the average newborn brain weight of 390g). The two plate-like brain hemispheres were lissencephalic, separated by shallow Sylvian fissures. Corpus callosum agenesis, large ventricles and small well-delineated basal ganglia and thalami were noted (Fig. 2c-e). These structural defects were accompanied by brain stem and cerebellum hypoplasia with small cerebellar folia (Fig. 3a). Dysmorphic facial features were noted including prominent occiput, absent fontanelle, large ears, wide nasal bridge, prominent upper lip, highly arched palate, cloudy corneas, right-sided single palmar crease and hypoplastic nails. There was renal aplasia with few primitive glomerular and tubular structures embedded in connective tissue and absence of ureters and bladder. These features were consistent with those observed during the pregnancy and birth of a previously affected female infant from the same pedigree who presented with microcephaly and renal agenesis, and survived only 4 hours following birth (Fig. 1b).

Family C is French and had no reported consanguinity. Proband C was born at full term with weight 2900g (-1 SD), length 46cm (- 2 SD), and a head circumference of 30cm (-3.5 SD) consistent with a diagnosis of microcephaly. Proband C has a sloping forehead, prominent nose, and relatively large ears. His neurological examination was remarkable for upper and lower limb hypertonia and brisk tendon reflexes in the lower limbs. He walked independently at 18 months of age. He has developmental delay with moderate to severe ID and mild autistic features. No metabolic, ERG or EEG abnormalities were detected. By age 10 years, his head circumference was 6.5SD below the age/sex mean and an MRI performed at 10 years of age showed a simplified gyral pattern and hypoplastic cerebellum (Fig. 2f-g). A second child in this

family (II:2) was also confirmed to have microcephaly by fetal MRI at 29 GWs (Fig. 2h-i). The biparietal diameter measured from the fetal MRI at that time was consistent with 23 GWs.

Whole exome sequencing (WES) and candidate gene screening were employed to identify a molecular diagnosis for these probands. Following WES for Family A (mother, father, proband and unaffected sibling), bioinformatics filtering removed common variants (minor allele frequency (MAF) >0.005). Annotated rare variants analyzed according to a consanguineous recessive mode of inheritance identified a homozygous G>A transition (c.1111+1 G>A; g. chr12: 120,260,623, hg19) disrupting the splice donor site of exon 9 in *CIT* (NM\_007174) (Fig. 1c). Sanger sequencing confirmed the presence of this mutation and its appropriate segregation in the family, with both parents being heterozygous carriers. *In silico* analysis of the exonic and intronic sequence flanking the c.1111+1 G>A nucleotide variant was evaluated with Human Splicing Finder (HSF) and identified cryptic splice donor sites 54 bp 5' of and 2 bp 3' of the abolished WT site (Supp. Fig 1a). A minigene reporter assay was used to assess alternative splicing. *CIT* WT and c.1111+1 G>A variant exon 9 were cloned into the pCAS2 reporter plasmid between pseudoexons A and B. Plasmids were transfected into HeLa cells to test cryptic splice site usage<sup>17</sup>. Sequencing the RT-PCR products confirmed that both cryptic splice donors are alternatives, with the splice site 2 bp 3' of the WT site most frequently used (Supp. Fig 1b,c). This major splice product results in a premature stop mutation in exon 10 that is predicted to undergo nonsense mediated decay. The spliced *CIT* transcript generated from the 54 bp 5' splice donor is a minor product and generates an 18 amino acid in-frame deletion in the kinase domain of CIT (CIT<sup>-18aa</sup>). The stability of mutant CIT<sup>-18aa</sup> has not been evaluated, but could disrupt kinase activity.

Resequencing of *CIT* coding exons and splice junctions in 35 probands with primary microcephaly identified two additional patients, Proband B and C, with recessive pathogenic

variants. A homozygous pathogenic mutation consistent with consanguinity was identified in Proband B. This 10bp deletion in exon 2 of *CIT*, creates a premature stop codon after 15 codons (NM\_007174; c.29\_38delATCCTTTGGA; g.chr12:120,313,935-120,313,944 hg19; p.Asn10Metfs\*15) and is predicted to function as a null allele (Fig. 1a,d). Proband C and Subject II:2 of Family C were found to carry compound heterozygous *CIT* variants. Both variants are located in the kinase domain; one generates a nonsense variant in exon 4 (c.412 C>T; g. chr.12: 120,295,329 hg19; p. Gln138\*) and one generates a missense variant in exon 5 (c.473 C>G; g. chr12: 120,288,021 hg19; p. Pro158Arg) (Fig. 1a,f). The p. Pro158Arg may express a partially functional protein that ameliorates the severity in the patient, compared with the homozygous null phenotypes in Probands A and B.

The *CIT* mutations presented here were absent from online genomic databases, including the 1000 Genomes Project, National Heart, Lung and Blood Institute (NHLBI) ESP6500, dbSNP 141, and the Exome Aggregation Consortium (ExAC) <sup>18-20</sup>. Bioinformatic variant annotation using SeattleSeq Variation Annotation revealed that the point mutations in our probands affect highly conserved bases with high GERP and CADD scores that are predicted to be pathogenic (Table 1) <sup>21,22</sup>. Further analysis of the genetic variation in *CIT* showed that loss-of-function alleles are infrequent. Fifteen heterozygous and no homozygous nonsense or frameshift alleles were present in the ExAC browser, and each had a frequency of <0.001. This suggests high evolutionary pressure against these alleles and supports the deleteriousness of the *CIT* variants. These findings correspond to a Residual Variation Intolerance Score (RVIS) of -2.35 indicating *CIT* is in the top 1.14% of genes in the genome intolerant to common functional genetic variation <sup>23</sup>.

Given the well established role for *CIT* in cytokinesis, our three cases implicate a novel pathogenic mechanism for microcephaly, a disorder previously linked primarily to gene products



that localize to the centrosome or mitotic spindle <sup>24</sup>. Severe microcephaly with widespread multinucleated neurons is characteristic of the structural and cellular pathology observed in the *Cit* knockout mouse and the *Flathead* rat (Supplemental table 1)<sup>10,11</sup>. In accordance with institutional research board and ethics committee approval, post-mortem analysis of Proband B allowed the human cell and molecular neuropathology associated with pathogenic variants in *CIT* to be analyzed. All non-neural tissue examined had normal cytology, but multinucleated neurons were observed throughout the neuraxis of Proband B, a hallmark of cytokinesis defects (Supplemental table 2). Microscopically, the profoundly microcephalic cerebral cortex showed both cytological and organizational abnormalities in many areas. The neocortex was excessively thick, with the six cortical layers replaced by a molecular layer and two broad layers comprised of loosely and irregularly scattered neurons (Fig. 2j,k). The underlying white matter was unmyelinated and contained scattered ectopic neurons. The overlying leptomeninges were greatly thickened with reticulin and collagen fibers, prominent vascularity, and heterotopic astrocytes and neurons, some of which were multinucleated (Fig. 2l). The hippocampi were dysplastic, small and under-rotated, with hypoplastic dentate gyri (Fig. 2m-o). Cortical hypoplasia and layer disorganization account for the recurrent spontaneous seizures associated with premature death in rodent models <sup>16</sup>. Extrapolating from these models, the cytoarchitectural abnormalities observed in Proband B are consistent with cytokinesis defects that contribute to reduced neuronal precursor proliferation, multinucleation of neurons and increased cell death. Despite the phenotypic similarities, pathogenic *CIT* variants have not been detected in epilepsy cohorts, including the Epi4K exome sequence collection of 264 epileptic encephalopathy trios <sup>25</sup>.

The cerebellar cortex of Proband B was hypoplastic and dysplastic (Fig. 3). Laminar disorganization was more evident in the hemispheres than the vermis, where folia were fused and Purkinje cells were observed in multilayered islands interspersed by abnormal granule cell domains (Fig. 3b-h). At birth, the external granule cell layer (EGL) is usually compact, with 4-6

rows of bipolar cells abutting the molecular layer (ML) (Fig. 3b,d,g). In Proband B the EGL was wider, the ML narrower, and were merged with the Purkinje cell layer (Fig. 3g-h). In this case the EGL was comprised of 2 or 3 compact rows of cells overlying a looser band of horizontally oriented, thin, elongated cell bodies, some clearly binucleate (Fig. 3e,f,h). Purkinje cells had short simplified dendritic arborization compared to controls and many were multinucleated (Fig. 3g-j). Likewise, the internal granular layer (IGL) was severely hypo-cellular (Fig. 3g-h).

In summary, we report the identification of pathogenic variants in *CIT* as a genetic basis for primary microcephaly and cerebellar hypoplasia, with phenotypic features remarkably similar to *Cit*<sup>-/-</sup> rodent models. These findings highlight the evolutionarily conserved function of CIT in neurodevelopment and the disproportionate sensitivity of the neuroaxis to pathogenic variants in this gene. Multinucleated neurons are rarely observed in the nervous system, apart from their occurrence in ganglion cell tumors. These genetic findings implicate novel mechanisms in the pathogenesis of primary microcephaly and allow us to describe the human presentation of this very interesting multinucleated neuronal phenotype.

## **Materials and Methods**

**Growth Standards** The Child Growth Standards published by World Health Organization were applied for weight, height and head circumference assessment. These standards can be found at <http://www.who.int/childgrowth/standards/en/>.

**DNA Extraction** DNA was extracted from peripheral blood lymphocytes for Family A and C using Qiagen Blood DNA extraction kit according to manufacturer's instructions. Proband B DNA was extracted from formalin-fixed, paraffin-embedded brain tissue using Qiagen QIAamp DNA FFPE Tissue Kit (Catalog Number 56404) per the manufacturer's instructions. Three independently extracted Proband B DNA samples were analyzed. Extracted DNA was

quantified with the use of Life Technologies Qubit dsDNA BR Assay Kit (Catalog Number Q32850) and a Qubit 2.0 Fluorometer.

**Whole exome sequencing** Quad family WES was performed for family A, including Proband A, father, mother and unaffected sibling. The exome was captured with in-solution Agilent SureSelect All Exon XT2 50 Mb Kit and sequenced with an Illumina HiSeq 2000 instrument at Beijing Genomics Institute, resulting in 97X coverage of more than 99% of the targeted exons. SNPs and indels were mapped and called with the SOAPAligner/SOAP2-SOAPSnP-BWA-GATK BGI analysis pipeline<sup>26,27</sup>. Reads were mapped against hg19, with an average of 65457 SNPs and 4455 Indels called per individual. Annotation, ranking, and stringent filtering of genetic variants was performed to exclude non-pathogenic variants with a MAF > 0.005 in dbSNP, 1000 Genomes, EVS or an in-house database. Nonsynonymous rare variants were filtered against reference databases and as potential candidates. Databases used for annotation include: CCDS (<https://www.ncbi.nlm.nih.gov/CCDS/CcidsBrowse.cgi>), RefSeq (<http://www.ncbi.nlm.nih.gov/refseq/>), Ensembl ([www.ensembl.org](http://www.ensembl.org)), and Encode ([www.encodeproject.org](http://www.encodeproject.org)). Variants were analyzed according to a recessive mode of inheritance.

**Candidate gene analysis** PCR primers for coding region amplification were designed using ExonPrimer from the UCSC Genome Bioinformatics Genome Browser (<http://genome.ucsc.edu/cgi-bin/hgGateway>) for assembly hg19. For Proband B, PCR reactions were prepared with Promega GoTaq Green Master Mix (Catalog #M712B), and products were cleaned up with Affymetrix ExoSAP-IT (Product Number 78201). The 46 coding exons of *CIT* on chromosome 12 were screened by dideoxy sequence analysis on an ABI 3730 sequencer (Applied Biosystems, Life Technologies), and sequence data was analyzed with Sequencher 5.1 (Gene Codes Corporation). Microcephaly gene panel testing for Proband C was paired with RainDance microdroplet PCR and 2X150bp sequencing with Illumina MiSeq. Deep sequencing

(142X) reads were mapped to hg19 with MiSeq analysis software and BWA-GATK with 99% coverage. Variants were filtered against MAF (>0.5%), dbSNP, 1000 Genomes, EVS and an in-house dataset. Rare variants were annotated for functional features of coding nucleotides with publically available databases outlined for WES.

**Online Databases** *CIT* variants identified were absent from 1000 Genomes Project (<http://browser.1000genomes.org>), National Heart, Lung and Blood Institute (NHLBI) ESP6500, NHLBI Exome Sequencing Project (ESP) Exome Variant Server (<http://evs.gs.washington.edu/EVS/>), dbSNP 141 (<http://www.ncbi.nlm.nih.gov/projects/SNP/>) and ExAC Browser (<http://exac.broadinstitute.org/>). SeattleSeq Variation Annotation 138 (<http://snp.gs.washington.edu/SeattleSeqAnnotation138/>) was used to generate GERP (Genomic Evolutionary Rate Profiling) conservation scores and CADD (Combined Annotation Dependent Depletion) scores. Alternative splicing was investigated with Human Splicing Finder version 3.0 (<http://www.umd.be/HSF3/HSF.html>). Residual Variation Intolerance Score was generated using <http://genic-intolerance.org>

### **Mini-gene Construction and Splicing Assay**

Functional analysis of splicing abnormalities caused by c.1111+1 G>A was performed using an *in vitro* minigene splicing assay according to previously published guidelines<sup>17</sup>. *CIT* exon 9 and approximately 150 bp of flanking intronic sequences were amplified from a control DNA sample and then cloned in the pCAS2 vector. The c.1111+1 G>A substitution was subsequently introduced using site-directed mutagenesis and analyzed for specific splicing abnormalities following transfection in HeLa cells. Forty-eight hours after transfection, transcriptional analysis was performed and the effect on splicing identified using RT-PCR and further confirmed using direct Sanger sequencing and agarose gel electrophoresis.

**Immunohistochemistry** Brain sections were examined with hematoxylin-eosin. Selected sections were stained with Kluver-Barrera, and immunostained for GFAP, 1:400 (Dako, Carpinteria, CA, #M0761), phosphorylated neurofilament NF-P, 1:10 (clone TA51, gift of Dr. J. Trojanowski, Hospital of University of Pennsylvania, PA), synaptophysin 1:100 (Dako, monoclonal #M7315) and calbindin 1:100 (monoclonal, Novocasta).

#### **Funding**

This work was supported by the National Institutes of Health (R00HD069624 to S.L.B).

#### **Acknowledgements**

We thank the families for their participation and contribution to this research. We appreciate Ritesh KC and Brian McGrath for stimulating discussion during manuscript preparation. Dr. Joseph Loturco provided feedback regarding *CIT*.

## References

1. Gilmore, E.C. & Walsh, C.A. Genetic causes of microcephaly and lessons for neuronal development. *Wiley Interdiscip Rev Dev Biol* **2**, 461-78 (2013).
2. Paridaen, J.T. & Huttner, W.B. Neurogenesis during development of the vertebrate central nervous system. *EMBO Rep* **15**, 351-64 (2014).
3. Bond, J. *et al.* ASPM is a major determinant of cerebral cortical size. *Nat Genet* **32**, 316-20 (2002).
4. Bond, J. *et al.* A centrosomal mechanism involving CDK5RAP2 and CENPJ controls brain size. *Nat Genet* **37**, 353-5 (2005).
5. Kumar, A., Girimaji, S.C., Duvvari, M.R. & Blanton, S.H. Mutations in STIL, encoding a pericentriolar and centrosomal protein, cause primary microcephaly. *Am J Hum Genet* **84**, 286-90 (2009).
6. Bilgüvar, K. *et al.* Whole-exome sequencing identifies recessive WDR62 mutations in severe brain malformations. *Nature* **467**, 207-10 (2010).
7. Guernsey, D.L. *et al.* Mutations in centrosomal protein CEP152 in primary microcephaly families linked to MCPH4. *Am J Hum Genet* **87**, 40-51 (2010).
8. Nicholas, A.K. *et al.* WDR62 is associated with the spindle pole and is mutated in human microcephaly. *Nat Genet* **42**, 1010-4 (2010).
9. Gauthier-Fisher, A. *et al.* Lfc and Tctex-1 regulate the genesis of neurons from cortical precursor cells. *Nat Neurosci* **12**, 735-44 (2009).
10. Sarkisian, M.R., Li, W., Di Cunto, F., D'Mello, S.R. & LoTurco, J.J. Citron-kinase, a protein essential to cytokinesis in neuronal progenitors, is deleted in the flathead mutant rat. *J Neurosci* **22**, RC217 (2002).
11. Di Cunto, F. *et al.* Defective neurogenesis in citron kinase knockout mice by altered cytokinesis and massive apoptosis. *Neuron* **28**, 115-27 (2000).

- 314 12. El Amine, N., Kechad, A., Jananji, S. & Hickson, G.R. Opposing actions of septins and  
315 Sticky on Anillin promote the transition from contractile to midbody ring. *J Cell Biol* **203**,  
316 487-504 (2013).
- 317 13. Green, R.A., Paluch, E. & Oegema, K. Cytokinesis in animal cells. *Annu Rev Cell Dev*  
318 *Biol* **28**, 29-58 (2012).
- 319 14. Gai, M. *et al.* Citron kinase controls abscission through RhoA and anillin. *Mol Biol Cell*  
320 **22**, 3768-78 (2011).
- 321 15. Bassi, Z.I. *et al.* Sticky/Citron kinase maintains proper RhoA localization at the cleavage  
322 site during cytokinesis. *J Cell Biol* **195**, 595-603 (2011).
- 323 16. Ackman, J.B., Ramos, R.L., Sarkisian, M.R. & Loturco, J.J. Citron kinase is required for  
324 postnatal neurogenesis in the hippocampus. *Dev Neurosci* **29**, 113-23 (2007).
- 325 17. Gaildrat, P. *et al.* Use of splicing reporter minigene assay to evaluate the effect on  
326 splicing of unclassified genetic variants. *Methods Mol Biol* **653**, 249-57 (2010).
- 327 18. Abecasis, G.R. *et al.* A map of human genome variation from population-scale  
328 sequencing. *Nature* **467**, 1061-73 (2010).
- 329 19. Psaty, B.M. *et al.* Cohorts for Heart and Aging Research in Genomic Epidemiology  
330 (CHARGE) Consortium: Design of prospective meta-analyses of genome-wide  
331 association studies from 5 cohorts. *Circ Cardiovasc Genet* **2**, 73-80 (2009).
- 332 20. Lek, M. *et al.* Analysis of protein-coding genetic variation in 60,706 humans. *bioRxiv*  
333 (2015).
- 334 21. Cooper, G.M. *et al.* Distribution and intensity of constraint in mammalian genomic  
335 sequence. *Genome Res* **15**, 901-13 (2005).
- 336 22. Kircher, M. *et al.* A general framework for estimating the relative pathogenicity of human  
337 genetic variants. *Nat Genet* **46**, 310-5 (2014).

- 338 23. Petrovski, S., Wang, Q., Heinzen, E.L., Allen, A.S. & Goldstein, D.B. Genic intolerance  
339 to functional variation and the interpretation of personal genomes. *PLoS Genet* **9**,  
340 e1003709 (2013).
- 341 24. Morris-Rosendahl, D.J. & Kaindl, A.M. What next-generation sequencing (NGS)  
342 technology has enabled us to learn about primary autosomal recessive microcephaly  
343 (MCPH). *Mol Cell Probes* **29**, 271-81 (2015).
- 344 25. Consortium, E.K. Epi4K: gene discovery in 4,000 genomes. *Epilepsia* **53**, 1457-67  
345 (2012).
- 346 26. Li, R. *et al.* SNP detection for massively parallel whole-genome resequencing. *Genome*  
347 *Res* **19**, 1124-32 (2009).
- 348 27. Li, R. *et al.* SOAP2: an improved ultrafast tool for short read alignment. *Bioinformatics*  
349 **25**, 1966-7 (2009).



352 **Table 1. Genetic and major clinical features**  
353

	Proband A	Proband B	Proband C	Subject II:2 of Family C
<b>C/T variant (hg19, NM_007174)</b>	Chr12: 120,260,623  c.1111+1 G>A	Chr12: 120,313,935 - 120,313,944  c.29_38delATCCTTTGGA  p. Asn10Metfs*15	Chr12: 120,295,329 and Chr12: 120,288,021  c.412 C>T and c.473 C>G  p. Gln138* and p. Pro158Arg	Chr12: 120,295,329 and Chr12: 120,288,021  c.412 C>T and c.473 C>G  p. Gln138* and p. Pro158Arg
<b>GERP Score</b>	5.900	N/A	4.660 and 5.280	4.660 and 5.280
<b>CADD Score</b>	31.000	N/A	38.000 and 27.800	38.000 and 27.800
<b>Gender</b>	Male	Male	Male	Male
<b>Gestational Length</b>	Full Term	Full Term	Full Term	Pregnancy terminated at GW 29+2
<b>Birth Weight</b>	2.6 kg (-2 SD)	1.730 kg (-4 SD)	2.92 kg (-1 SD)	N/A
<b>Birth Length</b>	Unknown (home birth)	27.2 cm (crown-rump -2.5 SD)	46 cm (-2 SD)	N/A
<b>Birth Head Circumference (HC)</b>	Unknown (home birth)	24 cm (-8 SD)	30 cm (-3.5 SD)	N/A
<b>HC at Most Recent Evaluation</b>	27 cm (-11 to -12 SD) measured at 3.5 months	N/A	43 cm (-6.5 SD) measured at 10.5 years	N/A
<b>Brain Abnormalities</b>	MRI revealed micro- lissencephaly, agenesis of corpus callosum, cerebellar and brainstem hypoplasia, and T2 hyperintensity of the whole white matter	Autopsy revealed micro- lissencephaly, absent corpus callosum, hindbrain and cerebellum hypotrophy, cerebral cortex hypotrophy, and comparatively large ventricles. Detailed neuropathology included in the main text.	Microcephaly (MRI not performed)	Fetal MRI revealed a microcephaly, biparietal diameter equivalent to a fetus of 23 WG, and gyration equivalent to a fetus of 26 WG
<b>Neurological Findings</b>	Upper and lower extremity hypertonia, axial hypotonia, increased DTRs, and spastic tetraplegia	N/A	Upper and lower extremity hypertonia, and brisk DTRs for the lower extremities	N/A
<b>Seizures</b>	No	N/A	No	N/A
<b>Intellectual Disability</b>	Not assessed	N/A	Moderate to severe ID with mild autistic features	N/A
<b>Development</b>	Delayed	N/A	Delayed	N/A
<b>Dysmorphisms</b>	Hypotelorism, sloping forehead, and relatively large ears	Prominent occiput, absent fontanelle, large ears, wide nasal bridge, prominent upper lip, high arched palate, cloudy corneas, a right-sided sinlge palmar crease and small nails	Sloping forehead, prominent nose, and relatively large ears	N/A
<b>Status</b>	Unknown	Deceased; one day after birth	Alive	Terminated pregnancy

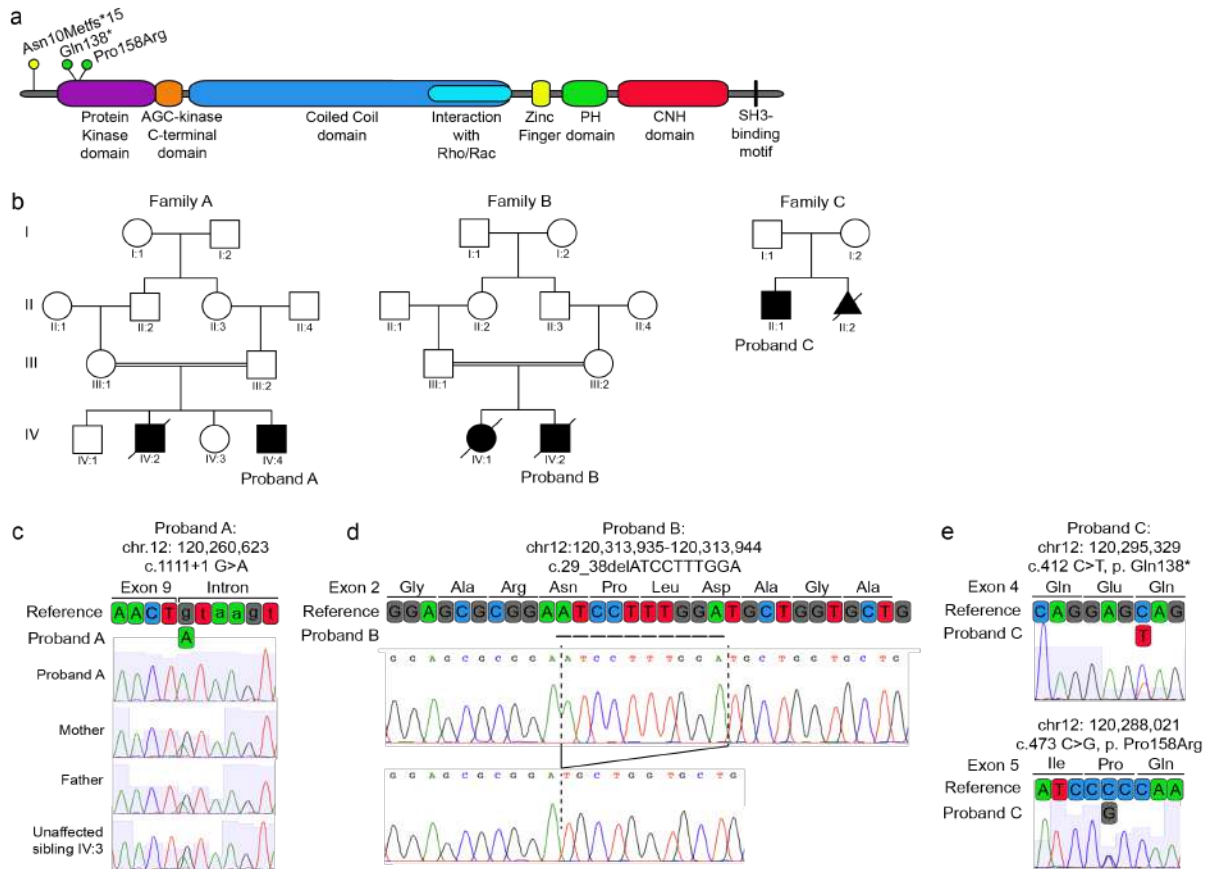


**Figure 1** Autosomal recessive *CIT* variants in micro-lissencephaly. (a) Protein domain organization of CIT showing pathogenic coding variants relative to protein domains. (b) Pedigrees of the families investigated with probands noted. (c) Chromatographs and schematic of the WT reference *CIT* exon 9/intron boundary, homozygous Proband A splice donor variant (c.1111+1 G>A) and cryptic splice donor site two bases downstream (boxed). Parents and unaffected sibling are heterozygous carriers. (d) Chromatograms defining the homozygous 10bp (c.29\_38delATCCTTTGGA) deletion in *CIT* exon 2 (chr12:120,313,935-120,313,944) amplified from Proband B that creates a stop after 15 codons (not shown). (e) Chromatographs and schematic of reference *CIT* exon 4 and exon 5 and the corresponding nonsense (c.412 C>T; p. Gln138\*) and missense (c.473 C>G; p. Pro158Arg) variants identified in Proband C.

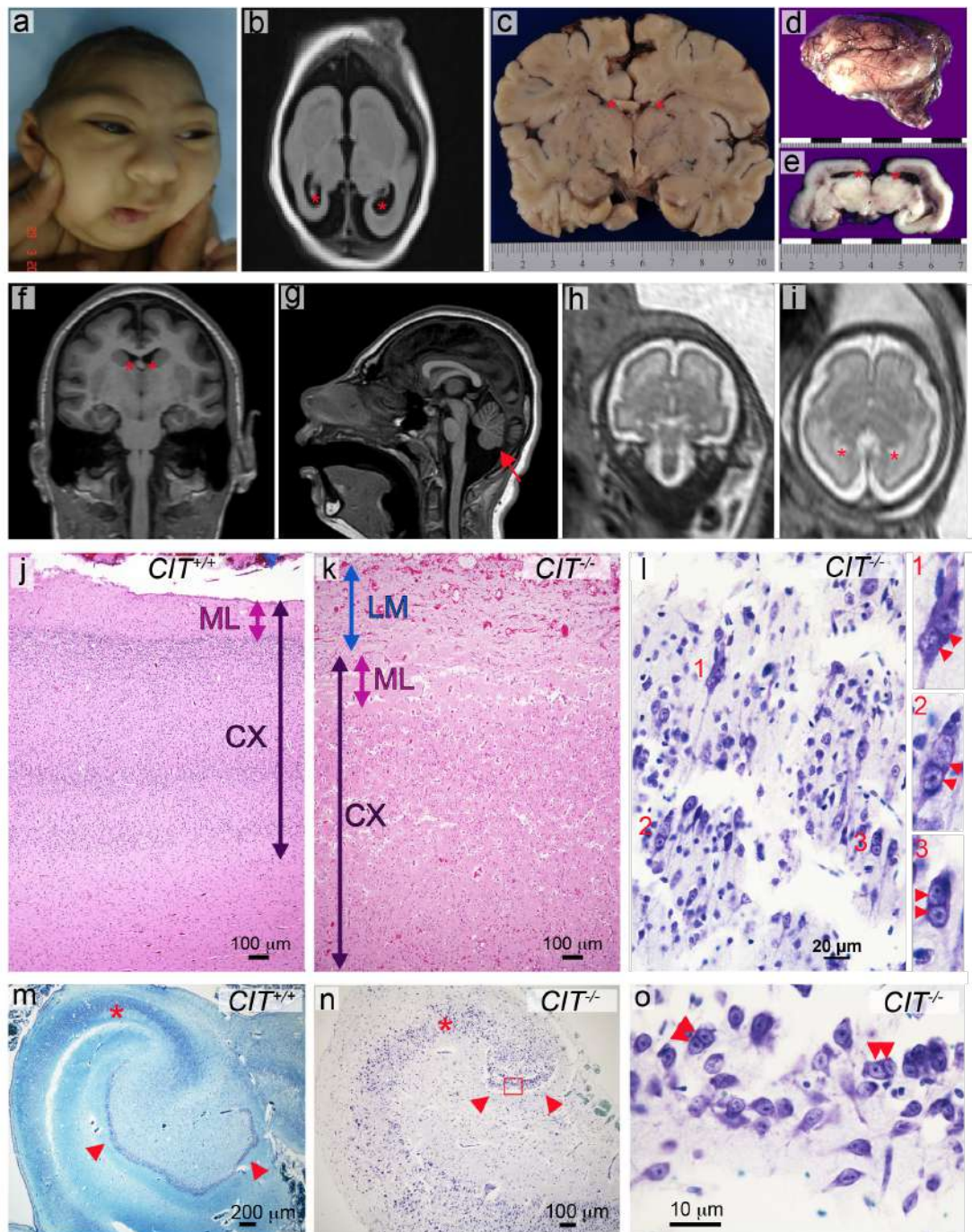


**Figure 2.** Structural and cellular neocortical phenotypes. (a) Proband A displays a microcephalic cranium, sloping forehead, wide nasal bridge and hypotelorism. (b) T2-weighted axial magnetic resonance imaging (MRI) of Proband A at 3.5 months. Cerebral cortical size is markedly reduced with simplification of gyral folding and enlarged ventricles (red asterisks). (c)

372 Coronal section of newborn control brain. Width is in centimeters (cm) and lateral ventricles  
373 marked by red asterisks. **(d)** Lateral view of lissencephalic newborn brain from Proband B (scale  
374 in cm). **(e)** Coronal section through mid-thalamus of Proband B brain showing enlarged lateral  
375 ventricles (red asterisks). **(f)** Coronal brain MRI of Proband C at 10 years of age showing  
376 microcephaly, simplified gyral pattern and enlarged ventricles (red asterisks). **(g)** Mid-sagittal  
377 Proband C MRI showing sloping forehead, hypoplastic brainstem and cerebellum (red arrow)  
378 **(h)** Coronal and **(i)** axial fetal brain MRI of affected subject II:2 of Family C at 29 GWs. Reduced  
379 brain volume, gyrification and enlarged ventricles (red asterisks) were noted. **(j)** Control and **(k)**  
380 Proband B cerebral cortex stained with hematoxylin and eosin (H&E). Compared to control **(j)**  
381 leptomeninges (LM; blue arrow) are excessively thick and contiguous with molecular layer (ML;  
382 pink arrow) in proband **(k)**. Cortex (CX; dark purple arrow) is thickened and cortical layering  
383 obscure when compared with control **(j)**. **(l)** High magnification of Proband B cortex stained with  
384 Kluver-Barrera. Disorganized parenchyma includes many multinucleated neurons: inserts show  
385 detail of multinucleated (red double arrowheads) cells labeled 1,2,3. **(m-n)** Kluver-Barrera  
386 stained sections of control **(m)** and Proband B **(n)** temporal lobe. The proband hippocampus **(n)**  
387 is very small with hypoplastic pyramidal layer (red asterisk) and greatly reduced dentate gyrus  
388 (arrowheads). Image of normal control hippocampus **(m)** imaged at half the magnification to  
389 allow for comparison of overall structure of the hippocampus. **(o)** Detail of Proband B dentate  
390 gyrus (red box in H), showing binucleated granule cells (double arrowheads).



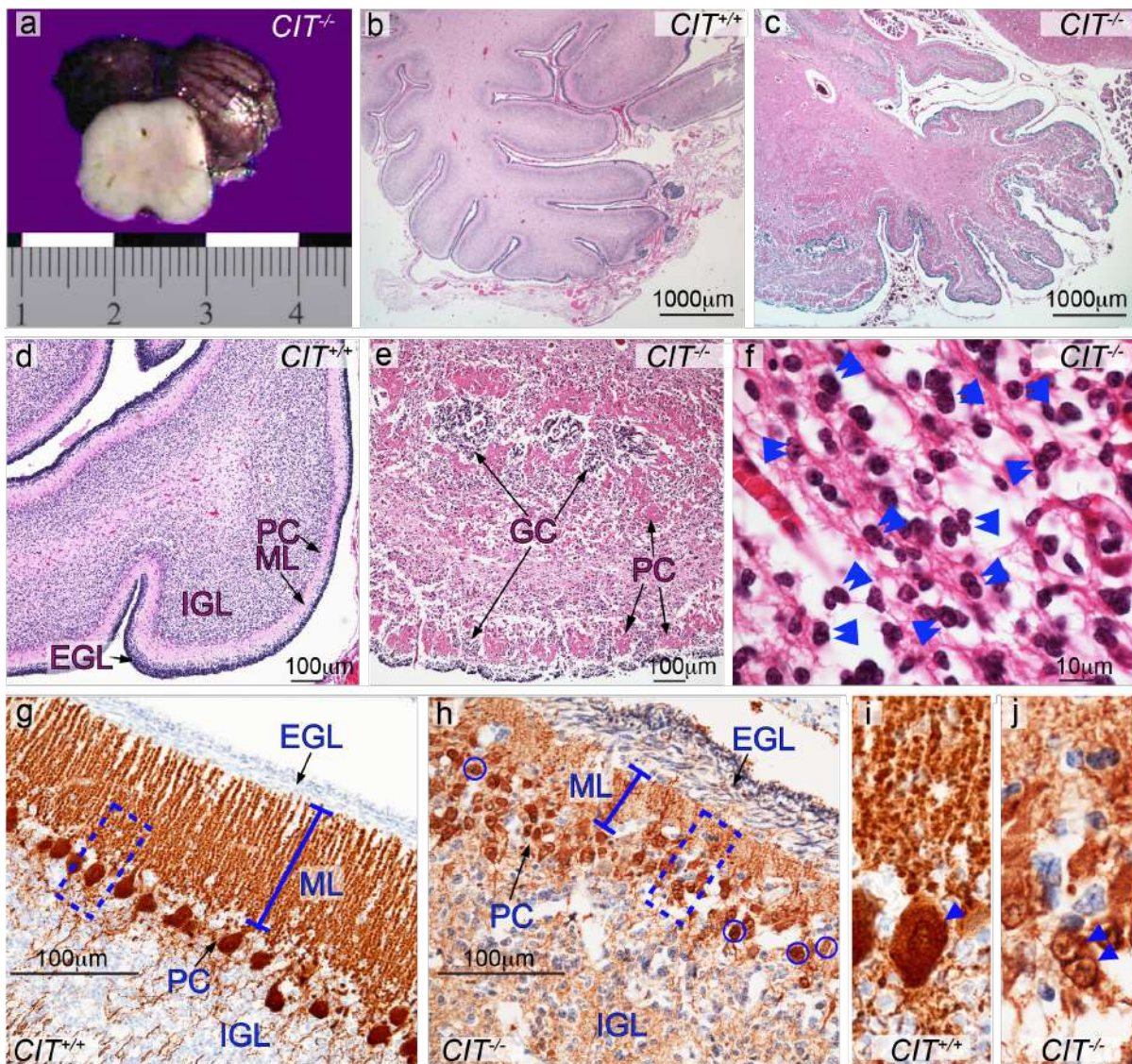
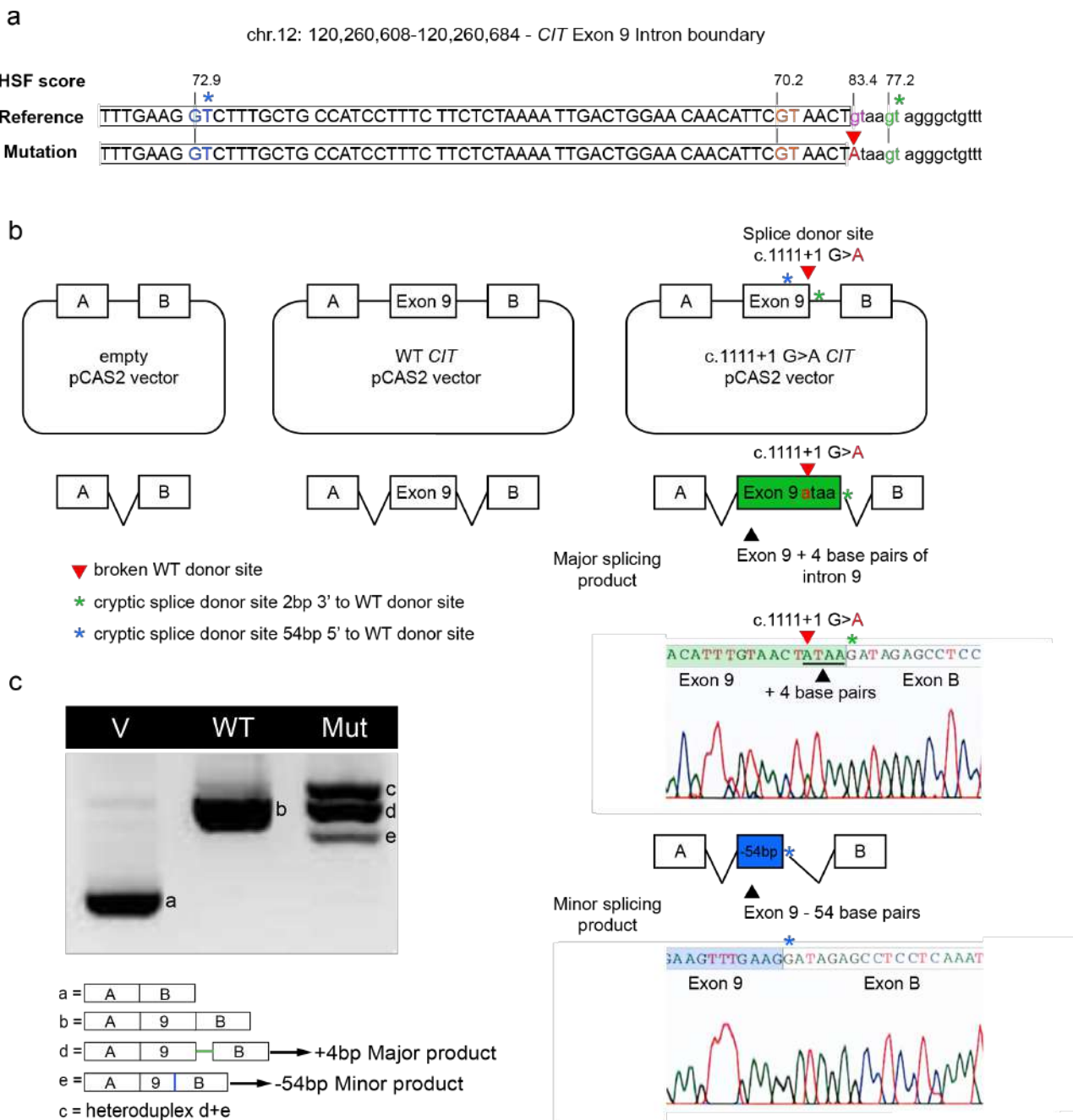


**Figure 3** Structural and cellular cerebellar *CIT* phenotypes. (a) Section through Proband B midbrain with external view of hypoplastic cerebellum. (b-f) histologic sections of cerebellum, stained H&E. Cerebellar folia are poorly developed and the cortex disorganized in Proband B (c,e & h). Cerebellar lamination in Proband B is disrupted with clustered Purkinje cells (PC) interspersed with granule cells (GC) within fused folia (c, e) as compared to control cerebellum (b, d). (f) Many GC appear binucleated (double blue arrowheads). (g-j) Cerebellum immunostained for calbindin shows abnormally thick EGL, reduced ML (blue line) and multilayered collections of small PCs (arrows) with stubby irregular dendritic processes in

400 Proband B (h), as compared with control (g). (i-j) Dashed boxes are enlarged to show  
401 binucleated PC (blue arrow heads) within a small soma in Proband B tissue (j) as compared to  
402 controls (i). EGL=external granule layer, IGL=internal granule layer, ML=molecular layer



404  
405  
406     **Supplemental Figure 1.** Alternative splicing between *CIT* exon 9 and pseudo-exon B (exon B)  
407     in minigene assay. Minigene splicing assay was performed according to previously published  
408     guidelines<sup>17</sup>. (a) Schematic of *CIT* sequence across the exon-intron border of *CIT* exon 9. WT  
409     (pink nucleotides) and cryptic splice sites (blue, orange and green nucleotides and asterisks)

410 were delineated and scored with Human Splice Finder (HSF). Exonic sequence is boxed and  
411 upper case. Intronic sequence is lower case. Proband A c.1111+1 G>A substitution (red  
412 arrowhead) breaks the WT splice donor site. (b) *CIT* exon 9 and approximately 150 bp of  
413 flanking intronic sequence was amplified from genomic DNA and cloned into the pCAS2 vector  
414 between pseudo- exon A and exon B. The c.1111+1 G>A substitution was introduced using  
415 site-directed mutagenesis. Forty-eight hours after transfection in HeLa cells, alternative spliced  
416 mRNA transcripts from empty (V), WT *CIT* exon 9 (WT), and c.1111+1 G>A *CIT* exon 9 (Mut)  
417 pCAS2 vectors were amplified by RT-PCR. (c) Differentially spliced products were detected by  
418 size separation on an agarose gel. Each product is labeled with a corresponding composition of  
419 the various splice products. Transcript composition was confirmed by Sanger sequencing. With  
420 loss of the WT splice donor, alternative splice transcripts were generated from nearby cryptic  
421 splice sites with the highest HSF scores. The major product included exon 9 along with an  
422 additional four base pairs of intron 9 (green asterisk and exon). The minor product includes only  
423 a portion of exon 9 with 54 base pairs excluded (blue asterisk and exon).



**Supplemental Table 1.** Mammalian models of null mutations in *CIT*.

Species	Proband B	<i>Cit</i> <sup>-/-</sup> Knockout Mouse (Di Cunto et al. 2000)	<i>Flathead fh/fh</i> Mutant Rat (Sarkisian et al. 2002) (Ackman et al. 2007)
<b><i>Citron</i> Kinase Mutation</b>	10 bp deletion in exon 2	Conditional excision exon 2 by <i>Cre</i> mediated homologous recombination	Spontaneous G/C bp deletion in exon 1
<b>Predicted Mutational Impact</b>	Frameshift causing a premature stop codon 25 amino acids from start site	Premature stop codon	Frameshift causing a premature stop 27 amino acids from start site
<b><i>CIT</i> Transcript</b>	Predicted NMD	NMD	NMD
<b>Brain Size and Weight</b>	Microcephalic and ~1/10 of the brain weight of an average newborn	Microcephalic 50% brain weight reduction	50% brain size reduction
<b>Cerebral Cortex Abnormalities</b>	Cortex shows low cellularity and disorganized three-layer arrangement. Presence of multinucleated neurons.	40% reduction in cerebral cortex thickness. Disorganized lamination of 6- layer cortex. Presence of binucleated cells.	Neocortex displays a reduced number of neurons but normal layering. Presence of binucleated neurons in neocortex.
<b>Cerebellar Abnormalities</b>	Global hypotrophy and disrupted laminar architecture. Crowded layer of Purkinje cells with simple dendrite projections. Binucleated Purkinje cells and granule cells.	70% cerebellum size reduction. Crowded layer of Purkinje cells with simple dendrite projections. Presence of binucleated cells.	Cerebellum displays a reduced number of neurons. Presence of binucleated neurons.
<b>Hippocampal Abnormalities</b>	Small and disorganized Ammon's horns. Only a small remnant of dentate fascia. Binucleated granule cells.	Normal Ammon's horn cell density and lamination. Essentially absent dentate gyrus.	Dentate gyrus displays a reduced number of neurons. Presence of binucleated neurons.
<b>Additional Locations of Multinucleated Cells</b>	Thalamus, striatum, brain stem and spinal cord	Thalamus	Striatum, thalamus, midbrain, hindbrain, and spinal cord
<b>Other Phenotypic Abnormalities</b>	Kidney and heart defects, facial dysmorphisms, and rotated lower limbs	Ataxia, seizures, and failure to thrive	Seizures and disrupted development of the retina

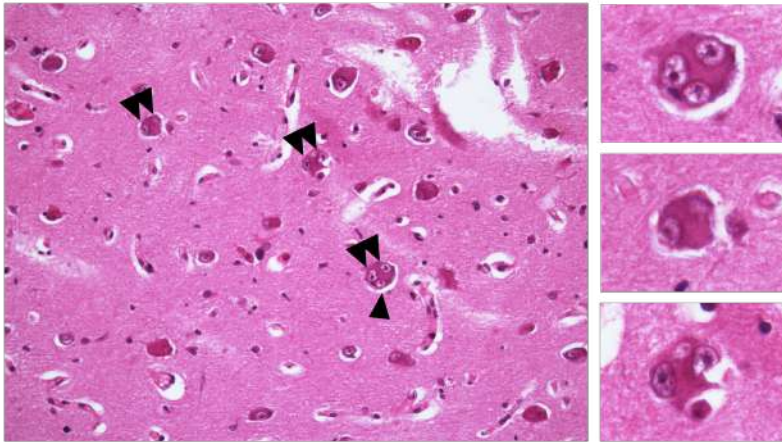
NMD=Nonsense mediated decay

428 **Supplemental Table 2.** Presence of binucleated neurons by anatomic area

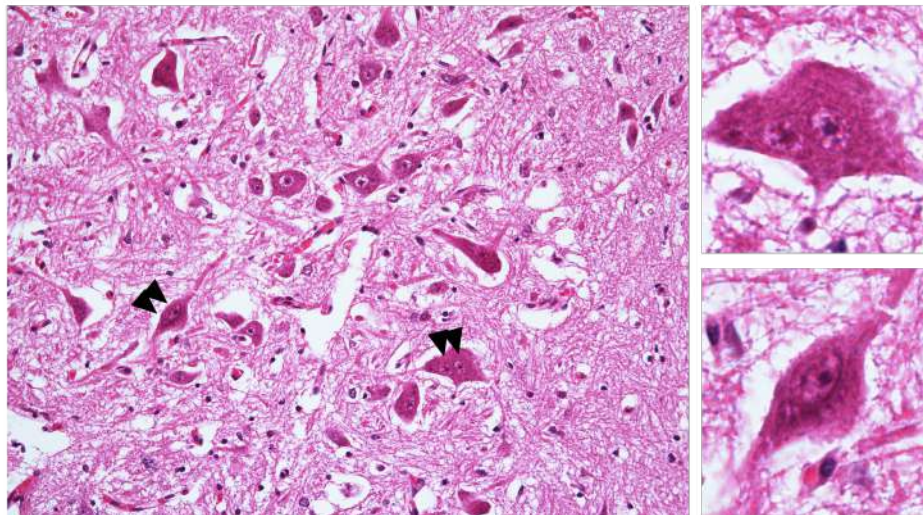
Presence of binucleated neurons by anatomic area	
<b>neocortex</b>	
<b>hippocampus</b> (pyramidal and granule cells)	
<b>thalamus</b>	
<b>striatum</b> (large and small cells)	
<b>pallidum</b>	
<b>cerebellum</b>	cerebellar cortex (Purkinje and granule cells)
	dentate nucleus
<b>brain stem</b>	midbrain tectum
	oculomotor nuclei
	pontine reticular formation
	nuclei pontis
	abducens nucleus
	inferior olive
	red nucleus
<b>spinal cord &amp; PNS</b>	anterior horn
	autonomic ganglion

429 PNS- Peripheral nervous system

a



b



430

431 **Supplementary Figure 2:** Multinucleated neurons throughout the neuraxis of the Proband B.

432 (A) Thalamus, (B) Spinal cord anterior horn. Cells indicated by arrowheads are enlarged in the

433 inserts and multinucleated.